

Article

Properties of Blue Phosphorene Nanoribbon-P3HT Polymer Heterostructures: DFT First Principles Calculations

Benita Turiján-Clara ¹, Julián D. Correa ², Miguel E. Mora-Ramos ^{1,*} and Carlos A. Duque ³

¹ Centro de Investigación en Ciencias-IICBA, Universidad Autónoma del Estado de Morelos, Cuernavaca CP 62209, Morelos, Mexico

² Facultad de Ciencias Básicas, Universidad de Medellín, Medellín 053108, Colombia; jcorrea@udemedellin.edu.co

³ Grupo de Materia Condensada-UdeA, Instituto de Física, Facultad de Ciencias Exactas y Naturales, Universidad de Antioquia UdeA, Calle 70 No. 52-21, Medellín 050010, Colombia

* Correspondence: memora@uaem.mx

Abstract: Recently, 2D phosphorus allotropes have arisen as possible candidates for technological applications among the family of the so-called Xene layered materials. In particular, the energy band structure of blue phosphorene (BP) exhibits a medium-size semiconductor gap that tends to widen in the case of using this material in the form of ribbons. BP nanoribbons have attracted recent interest for their implication in the improvement in efficiency of novel solar cells. On the other hand, compound poly (3-hexylthiophene) (P3HT) is used as the semiconducting core of organic field effect transistors owing to such useful features as high carrier mobility. Here, we theoretically investigate the electronic properties of a heterostructure combination of BP—in the form of nanoribbons—with a P3HT polymer chain on top in order to identify the features of band alignment. The work is performed using first principles calculations via DFT, employing different exchange correlation approaches for comparison: PBE, HSE06 and DFT-1/2. It is found that, under DFT-1/2, such a heterostructure has a type-II band alignment.

Keywords: P3HT; blue phosphorene; nanoribbons; DFT



Citation: Turiján-Clara, B.; Correa, J.D.; Mora-Ramos, M.E.; Duque, C.A. Properties of Blue Phosphorene Nanoribbon-P3HT Polymer Heterostructures: DFT First Principles Calculations. *Condens. Matter* **2023**, *8*, 74. <https://doi.org/10.3390/condmat8030074>

Academic Editors: Alexey Kavokin and Helgi Sigurdsson

Received: 30 June 2023

Revised: 16 August 2023

Accepted: 19 August 2023

Published: 22 August 2023



Copyright: © 2023 by the authors. Licensee MDPI, Basel, Switzerland. This article is an open access article distributed under the terms and conditions of the Creative Commons Attribution (CC BY) license (<https://creativecommons.org/licenses/by/4.0/>).

1. Introduction

After the discovery of graphene [1], the materials science community embarked on the search for other potential systems with two-dimensional crystal structures [2]. Among the various graphene-like materials discovered are those composed of atoms of a single chemical element. These have been called Xenens, based on the ending of their names (silicene, stanene, borophene, antimonene and others) [3], all of them produced artificially. This class of materials exhibits remarkable prospects for electronic integration as well as promising applications in optics and photonics [4]. One standout in this group is phosphorene, a layered allotrope of phosphorus with semiconductor properties. Among the experimentally obtained structural phases of phosphorene are black phosphorene (α -P or, simply, phosphorene) and blue phosphorene (β -P, referred to hereafter as BP) [5]. The latter was theoretically proposed by Zhu and Tománek in 2014 [6]. Various reports of its experimental realization have shown its synthesis through epitaxial methods on Au(111) substrates [7–10]. However, achieving BP growth through this approach continues to face considerable challenges. On the other hand, theoretical studies employing different approaches have been more abundant in the literature. To cite a couple of recent examples, Shaikh et al. conducted first principles calculations of its electronic, optical and vibrational properties [11], and a simulation in the same spirit proposed to employ monolayer BP as a high-mobility channel, while bilayers of BP would serve as metallic electrodes, in a model for junction-free field-effect transistor [12].

Very recently, the use of first principles methods has identified a plausible route for the mass production of this promising material in an epitaxial form on Ag(111) [13]. The simulation employs density functional theory (DFT) calculations, subsequently validated by molecular dynamics, to explain the growth of single-crystal layers from BP nanoribbons that gradually evolve into a monolayer. In fact, the present work focuses on BP nanoribbons. Initial studies on their properties date back to the very year 2014 when Xie et al. analyzed the effect of quantum confinement on the band structure of nanoribbons with zigzag and armchair edge configurations [14]. In both cases, the use of DFT allowed the identification of these systems as indirect gap semiconductors, with the bandgap decreasing as the nanoribbon width increases.

Since that date, numerous studies have been dedicated to investigating BP nanoribbons. To mention some of the works involving first principles DFT calculations, Liu and collaborators analyzed the magnetic and spin properties of zigzag nanoribbons [15]. The effect of electric fields on the electronic structure and optical response of such nanoribbons were explored [16], and a semiconductor-to-metal transition can occur in them due to the presence of a giant Stark effect, as reported in Ref. [17]. A study on the influence of electric fields on edge states is presented in [10]. DFT calculations have identified tunable electronic and dielectric properties in ultra-narrow BP nanoribbons [18], while theoretical investigations within the same formalism regarding transport properties in these nanosystems indicate the possibility of controlling them through edge passivation with different groups [19]. Similarly, the effect of edge corrugation in zigzag BP nanoribbons is predicted as a tool for bandgap engineering, leading to their increase and transition to a direct character [20]. As for applications, various reports mention a variety of possibilities. The sensing of organic molecules using BP nanoribbons is investigated in the work by Saravanan et al. [21]. The functionalization of edges in these structures enables them to act, for instance, as novel catalysts for water splitting [22]. Additionally, the inclusion of BP nanoribbons has contributed to improving the efficiency of perovskite-based photovoltaic cells by enhancing hole extraction and increasing hole mobility [23].

The adsorption and doping of BP involving atoms of other chemical elements have also been subjects of investigation using first principles methods. The substitution of BP atoms with light non-metallic elements such as B, C, N, O and F was considered in the work by Sun et al. [24]. The report by Ding et al. examines the adsorption of metallic and non-metallic atoms on black phosphorene and BP [25]. Tuning the electronic and magnetic properties of BP through doping with Al, Si, As and Sb has been proposed [26]. The influence of other atoms from groups IV and VI, as well as various metallic atoms, acting as dopants in BP, has also been investigated [27,28]. In the case of BP nanoribbons, Correa has reported calculations of optoelectronic properties considering doping with C, Si and S for both zigzag and armchair configurations [29].

Poly 3-hexylthiophene (P3HT) is a conjugated semiconductor polymer that shows a strong tendency to crystallize, forming ribbon-like nanostructures, and can be fabricated in the form of thin films [30,31]. It is easy to synthesize and exhibits good optoelectronic properties, which have allowed its application in various organic electronic devices, such as solar cells, organic field effect transistors (OFETs), light-emitting diodes and others [32]. Within the field of 2D materials, P3HTs have been blended to graphene nanoribbons to produce OFETs, which show a three-fold increase in the charge carrier mobilities when compared to pure P3HT devices [33]. Similarly, OFETs have been fabricated using doped MoS₂ nanosheets as the active layer, combined with P3HT films, resulting in a significant improvement in the polymer's mobility compared to undoped P3HT [34]. For the sake of photovoltaic applications, electronic and optical properties of combinations of P3HT with organic [35,36] and inorganic systems [37] have been investigated. In particular, the work in [37] dealt with Heyd–Scuseria–Ernzerhof (HSE) hybrid-functional DFT calculations of electronic and structural features of P3HT–PbS and P3HT–CdS hybrid interfaces. It is also relevant to mention a recent theoretical and experimental study that investigates the band alignment between P3HT and exfoliated multilayers of black phosphorene. Among other

properties, a remarkable charge delocalization from the polymer towards the conduction band of black phosphorene was observed [38].

These recent references point to a growing interest in organic 2D inorganic hybrid heterostructures. For this reason, as previously mentioned, the objective of this study is to explore the basic electronic properties of the heterojunction between BP nanoribbons and P3HT films. The investigation, of a theoretical nature, will be conducted using DFT. Aside from the DFT-1/2 approach, we shall employ, for the sake of comparison, GGA+PBE and HSE06 calculations for both BP and P3HT systems. This is conducted in order to discuss the validity of the results obtained by means of the computationally cheaper DFT-1/2 approach. In the following section, we will discuss in detail the simulation tool employed. Subsequently, the obtained results will be presented, and the conclusions of the study will be outlined.

2. Computational Methodology

In 2008, Ferreira, Marques and Teles introduced an approximation within DFT in order to develop a cheaper way of improving the calculation of energy band gaps in semiconductors, compared to the typical underestimation achieved within LDA or GGA [39,40]. It was named DFT-1/2. The authors used Slater's half-occupation DFT technique [41,42] together with exchange correlation approximations to suitably modify DFT approach for band gap rectification. They show that, even when the technique might not be entirely convenient, obtained results are much better than the outcome from LDA and GGA. Here, we shall employ the GGA-1/2 variant of this approach, as implemented in the open access code SIESTA [43,44]. This package of first principles calculations employs a linear combination of localized atomic orbitals (LCAO). Our procedure includes polarized double- ζ basis and norm-conserving pseudopotentials. Relaxation in the cell is sought until the residual force on each atom becomes smaller than 0.02 eV/Å. A mesh cutoff energy of 250 Ry guarantees the energetic convergence. After reaching it, calculation of electronic and optical properties uses a $10 \times 10 \times 1$ Monkhorst–Pack partition mesh of the Brillouin zone. In the case of the supercell, this partition is $3 \times 3 \times 1$.

As mentioned, sole GGA+PBE [45] as well as hybrid-functional HSE06 [46–48] approaches are also employed to determine the band structure of involved compounds: the P3HT polymer and the BP nanoribbon (BPNR). The first is implemented through SIESTA, with the same parameterization, while the second is carried out with the GPAW environment, with a basis of plane waves having an energy cutoff of 650 eV, and a possibility of using finite difference to solve the Poisson equation and calculate the exchange correlation potential [49,50]. This is completed in order to compare results and, at the same time, contribute to discuss the suitability of the use of SIESTA-based DFT-1/2 formalism for the calculations of interest. For example, it is widely known that describing exchange and correlation through hybrid HSE06 functional leads to estimations of semiconductor energy band gap in semiconductors closer to the accepted experimental values [51].

3. Results and Discussion

Figure 1 contains schematic views of the systems investigated. The P3HT 1D oligomer chain design that leads to the periodic chain used to combine with BP nanoribbons appears depicted in Figure 1a (shown with $N = 4$ dimer units). The view of the zigzag nanoribbon configuration with 10 hexagonal units of width (NRZ-10) is shown in Figure 1b, with H-passivated edges. The unit cells for the two distinct configurations considered in the case of the P3HT–BP nanoribbon heterostructure appear in Figure 1c,d for the side-on and edge-on orientations of the 1D P3HT periodic polymer chain, respectively (here, we use the same terminology as Ref. [38]).

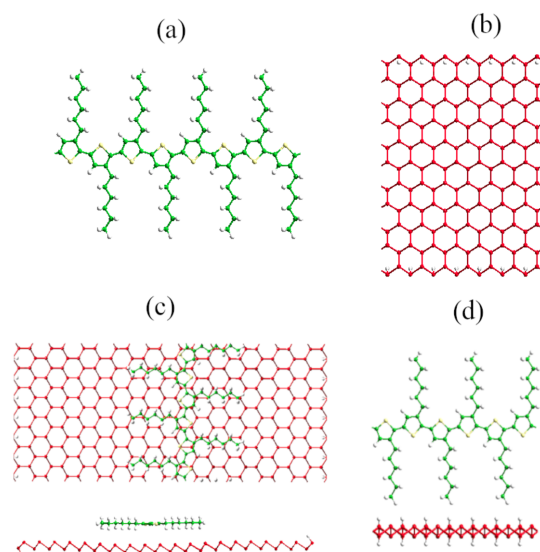


Figure 1. (Color online) (a) View of the P3HT oligomer. Carbon atoms are shown in green color, hydrogen atoms in white and sulfur ones in yellow. (b) Schematic view of a zigzag blue phosphorene nanoribbon with 10 hexagon units of width (phosphorus atoms are in red color). (c) Upper view of the unit cell of the complex blue phosphorene nanoribbon plus 1D P3HT chain with side-on configuration. The growth of the heterostructure proceeds along the vertical axis. (d) Lateral view of the unit cell of the complex blue phosphorene nanoribbon plus 1D P3HT chain with edge-on configuration. The growth of the heterostructure proceeds along the horizontal axis.

3.1. P3HT Oligomers and Periodic Chain

We have calculated the HOMO–LUMO energy difference for several P3HT oligomers consisting of N dimer units (D- N). The evolution of such quantity is presented in Figure 2. They were obtained under GGA+PBE (both using SIESTA and GPAW), DFT-1/2 (SIESTA) and hybrid HSE06 (GPAW) numerical approaches. In the crystal limit, the value of the direct energy band gap for the infinite polymer chain is plotted as well, indicated by the P3HT label at the right side of the horizontal axis. In all cases, there is a decreasing tendency of this energy difference towards the periodic result. The GGA+PBE values obtained within the two platforms are almost identical. The decreasing tendency of the HOMO–LUMO gap here obtained coincides with DFT calculations performed using Becke’s three-parameter exchange functional along with the Lee–Yang–Parr nonlocal correlation functional (B3LYP) [52]. However, the HOMO–LUMO gaps there reported are significantly larger than those here obtained. As expected, hybrid-functional HSE06 provides for larger estimation, as also results from employing DFT-1/2. However, the latter leads to a higher energy band gap for the polymer dimeric crystal chain: $E_{gP3HT} = 1.62$ eV. This value lies within the intense part of the solar spectrum. Hence, it might indicate potential usefulness in power conversion efficiency. Moreover, for the sake of comparison, we plot the values of energy gap for the P3HT polymer chain presented in several previous works, including bilayer cases [37,52–54]. Interestingly, our PBE and HSE06 calculations for the polymer chain are close to those obtained by other groups for bilayer structures, but it is worth noticing that those results correspond to systems where there are either PbS or CdS layers underlying the P3HT polymer [37]. In relation to this fact, one must keep in mind that most experimental energy gap reports largely depend on the substrate onto which the polymer thin film is deposited. In this sense, in the same work by Ansari et al. [52], the authors discuss experimental measurements of spectroelectrochemistry, cyclic voltammetry and optical spectroscopy for a solid thin film of P3HT chains with six monomer units on indium tin oxide (ITO). This was completed in order to study electric and optical energy band gaps. Accordingly, the electrical gap was determined to be equal to 1.96 eV, whilst the optical gap

was found to be 2.46 eV. The first of those values lies in between our D-3 and D-4 oligomer DFT-1/2 results.

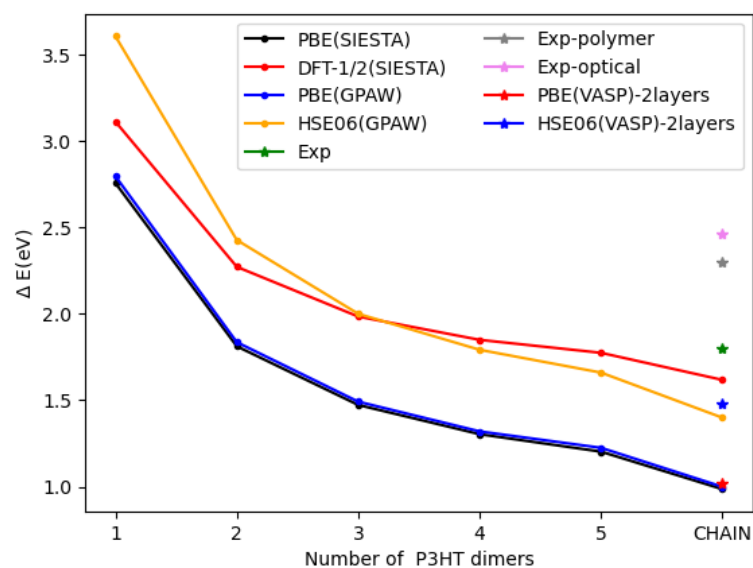


Figure 2. (Color online) Evolution of HOMO–LUMO energy gap as a function of the size of P3HT oligomers constructed with dimer units (see Figure 1a). Results were obtained using DFT–PBE, calculated under both SIESTA and GPAW environments, and with DFT(PBE)-1/2 implemented in SIESTA. HSE06 under GPAW are shown as well. The rightmost value in each case indicates the limit of periodic chain (energy band gap). Labels used to identify polymer gaps in the inset correspond to the following references: *Exp* [54], *Exp-polymer* [53], *Exp-optical* [52], *PBE-2Layer* and *HSE-2Layer* [37]

At this point, it is worth discussing the outcome of the DFT-1/2 approach in this case. As is known, this method mostly relies on a suitable choice of a certain cutoff radius for the ions involved in the compound. Here, following the work of García-Basabe et al., we have only modified this parameter for C atoms, leaving H and S ones untouched. This is justified by the predominant influence of carbon p-orbitals in determining the valence band properties in the polymer [38]. However, we have not only sought maximizing the electronic band gap of P3HT but also tried to reproduce as much as possible the features of its energy band structure. For that reason, our choice for C cutoff radius is 5.4 Bohr instead of the 3.8 Bohr value chosen in [38]. Similarly to what was completed in that work, we switched to 1/4 description (instead of 1/2) for the charge ionization. Our selection can be justified by observing the calculated P3HT band diagram presented in Figure 3. There, the electronic structure is plotted, comparing GGA+PBE, HSE06 and DFT-1/2. It is readily noticed that HSE06 maintains the overall behavior of the band structure compared to GGA+PBE and mostly acts by enhancing the direct band gap. In the case of using DFT-1/2, our choice of parameters provides a quite correct description of both valence and conduction band features when compared to the other approaches used at the time that E_{gP3HT} becomes enhanced. In this sense, our use of the DFT-1/2 approach is meant to reach a balance between enhancing the energy gap and fairly reproducing the band structure of the polymer.

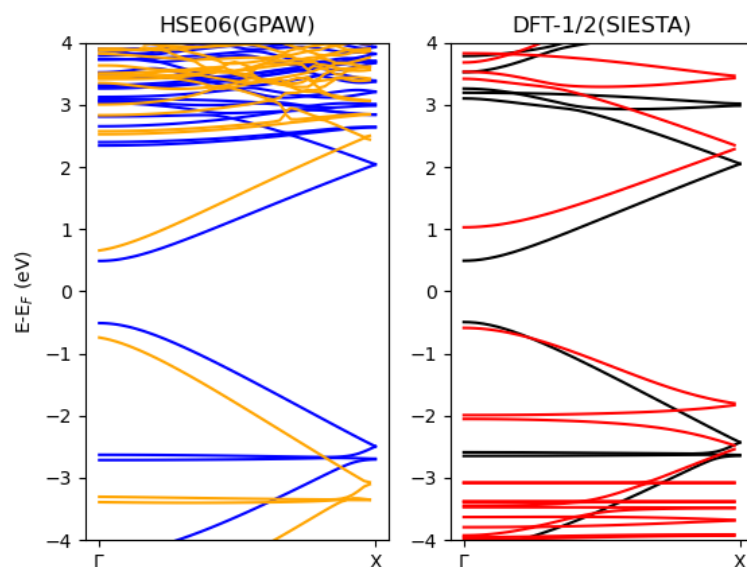


Figure 3. (Color online) Calculated energy band structure of P3HT periodic polymer chain. (Left panel) calculated under GPAW with GGA+PBE (blue, thinner, lines), and HSE06 hybrid functional (orange, thicker, lines). (Right panel) calculated under SIESTA, with GGA+PBE (black lines) and DFT-1/2 (red lines).

3.2. Blue Phosphorene Nanoribbons

The same numerical approaches above employed have been used to calculate the energy band structure of BP zigzag nanoribbons with H-passivated edges. The variation in band gap as a function of the ribbon width appears depicted in Figure 4.

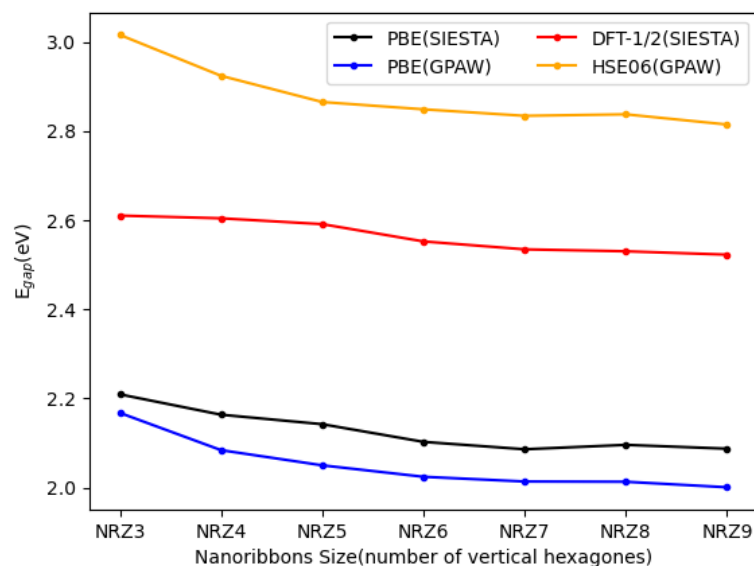


Figure 4. (Color online) Evolution of energy band gap of zigzag blue phosphorene nanoribbons as a function of ribbon width, indicated by NRZ-K, with K numbering the hexagonal units along the transverse ribbon direction. Results are presented for GGA+PBE under SIESTA and GPAW, DFT-1/2 under SIESTA and hybrid HSE06 under GPAW.

In general, a decreasing behavior of BP nanoribbon band gap is revealed within all first principles approaches used. GGA+PBE yields distinct functional variations, with the GPAW-based one having the smaller results. In all cases, E_{gBPNR} remains above 2 eV, but HSE06 seems to somehow overestimate the band gap, although a previous report

presents a HSE06 gap of 2.67 eV for the monolayer, which might be close to the limiting value of the extended 2D BP in our case [55].

DFT-1/2 produces the slightest decreasing trend of all. It is directed towards our calculated 2D monolayer band gap value of $E_{gBP} = 1.97$ eV, which agrees with the accepted result of 2.0 eV [56].

This time, the choice of cutoff radius in the case of P atoms also took into account, besides achieving a maximum possible gap value for all ribbon widths considered, the correct reproduction of the main features of energy bands in the systems. It turns out that the same value used in Ref. [38] for the calculation of the energy structure of black phosphorene monolayers leads, here, to seemingly correct results. So, we have used a P cutoff radius of 3.3 Bohr, with 1/4 ionization.

In accordance, for the sake of illustration, we present in Figure 5 the calculated electronic structure of NRZ-8 BP nanoribbon using the named four different first principles approaches. It can be noticed that the outcome of DFT-1/2, with the mentioned choice of parameters, closely resembles the band diagrams arising from GGA and HSE06 schemes regarding the morphology of valence and conduction dispersion relations. The GGA+PBE and DFT-1/2 schemes yield a barely indirect energy band gap in the case used as an example. Interestingly, the HSE06 calculation provides a direct band gap at the Brillouin zone center.

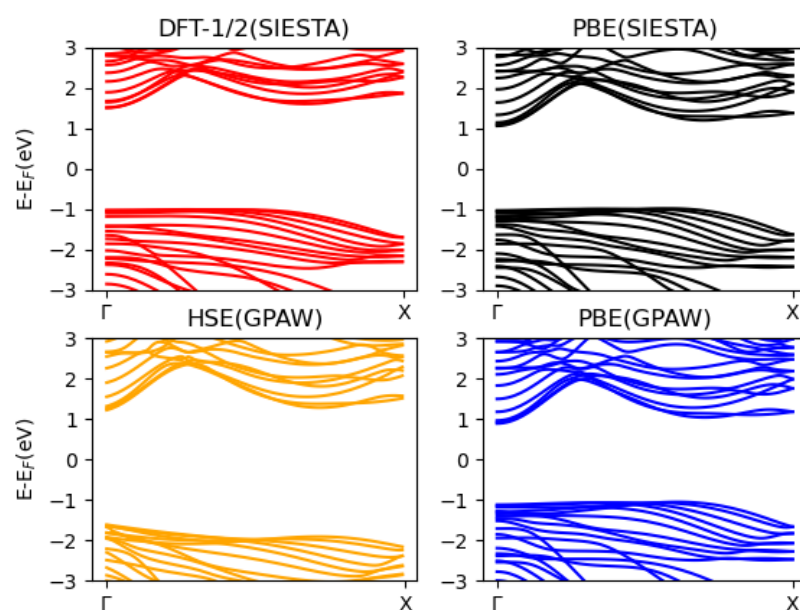


Figure 5. (Color online) Calculated energy band structure for the NRZ-8 zigzag blue phosphorene nanoribbon. Results for different DFT-based first principles approaches are used. The right column contains GGA+PBE band structures under SIESTA and GPAW environments. Left column shows the outcome of DFT-1/2 (SIESTA) and HSE06 hybrid functional (GPAW) procedures.

3.3. The Blue Phosphorene Nanoribbon plus P3HT Complex

The previously presented results pave the way for the calculation of the electronic properties of the heterostructure formed when a periodic 1D P3HT polymer chain is placed on top of a BP zigzag nanoribbon, as is schematically depicted in Figure 1c,d. The design chosen for such an arrangement contemplates the location of a polymeric chain just above the middle longitudinal axis of the ribbon. For on-edge configuration, this can be achieved for all the ribbon widths considered. When the P3HT chain is put side-on, the width of the ribbon has to be extended beyond the lateral extension of the dimer (vertical size of Figure 1a).

Figure 6 contains the calculated band structures of BP (H-passivated) zigzag nanoribbon plus 1D P3HT periodic chain complexes. First, the results for different ribbon widths and

edge-on polymer chains are depicted. The immediate conclusion is that the whole system behaves as a direct narrow gap semiconductor. For the examples depicted, the gap values range from 0.14 eV to 0.18 eV. There is little difference when comparing the band diagrams of complexes with equal ribbon widths but with side- and edge-on P3HT chain orientations for wide-enough underlying BPNR. This can be observed from the plots in the lower row of the figure. Here, the case of NRZ-19 is considered for illustration.

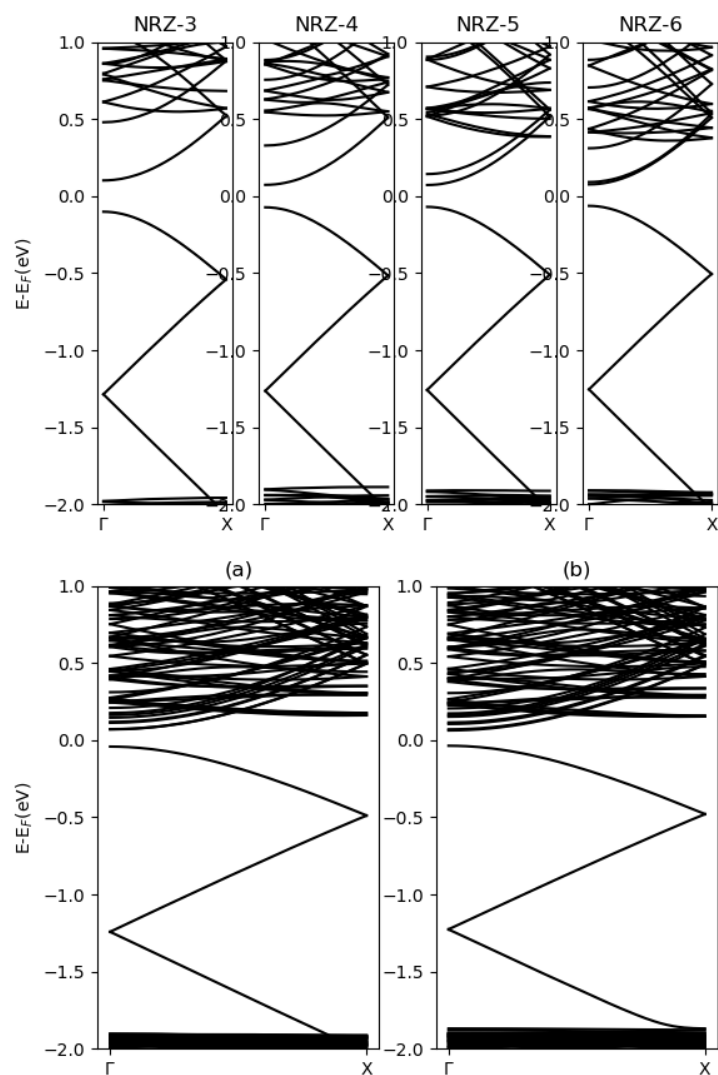


Figure 6. (Upper panel) Energy band structure of the complex P3HT 1D periodic chain plus blue phosphorene zigzag nanoribbon, with edge-on geometric configuration (see Figure 1d). Different ribbon widths are considered, indicated by K number of hexagonal units in the NRZ-K labels on top of the plots. In all cases, zero energy values correspond to Fermi level. (Lower panel) (a) Energy band structure of P3HT periodic chain plus zigzag blue phosphorene for the side-on case of Figure 1c, which corresponds to $K = 19$; (b) the same for the edge-on geometric configuration of Figure 1d, with equal ribbon width.

We have also analyzed how the alignment of P3HT polymer onto the nanoribbon affects the electronic structure of the complex. With that purpose, we again choose the wide-enough NRZ-19 and consider a shift in the side-on P3HT chain from on-center position towards one of the passivated ribbon edges. Figure 7 presents five different alignments between the P3HT chain and NRZ-19, as well as the resulting electronic structures. Our findings indicate that the alignment of P3HT with the nanoribbon does not cause significant

changes in the electronic structure near the Fermi level, such that the disposition of the band's edges is practically independent of the complex alignment.

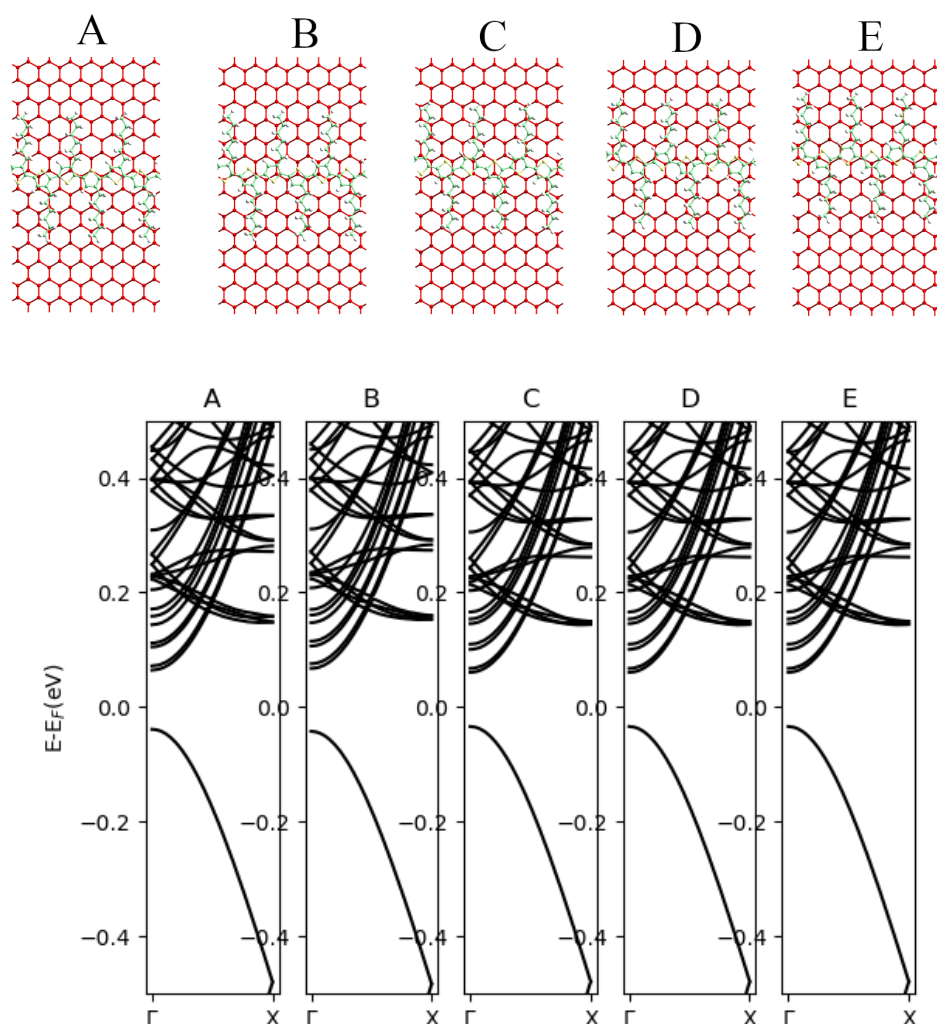


Figure 7. (Upper panel) Schematic representation of five different alignments between P3HT and NRZ-19. (Lower panel) Bands structure of the five alignments considered in upper panel. The alignments are labeled as (A–E).

Viewing our system as a heterostructure formed by putting together a BP zigzag nanoribbon and a 1D P3HT periodic polymeric chain, the subject of main interest is the kind of band alignment achieved. This feature will determine the charge carrier properties in the system. Here, we choose to evaluate, via DFT-1/2, this alignment in the case of edge-on configuration. Our results point at a type-II band alignment as depicted in Figure 8. There, the positions of conduction band minimum and valence band maximum of each component are depicted for several values of the zigzag nanoribbon widths. This result contrasts with the P3HT+black-phosphorene heterostructure reported in Ref. [38]. There, the edge-on configuration exhibits a type-I band alignment.

In addition, the two rightmost plots in Figure 7 represent the band alignment for the heterostructure formed regarding the wide BP NRZ-19. In one case, only one polymer chain is assumed to be forming the heterostructure. In the other, the ribbon width is completely covered by three parallel adjacent side-on P3HT chains. In both cases, the type-II arrangement is maintained, but, in the second one, it is possible to notice a greater separation between aligned bands. Actually, the incorporation of more P3HT chains causes a relative descent in polymer energies and a rise in ribbon ones. We attribute this effect

to the increment in charge transfer between layers, but further analysis would be needed to confirm this assumption, considering whether there is a real possibility for practical realization of such kind of heterostructure.

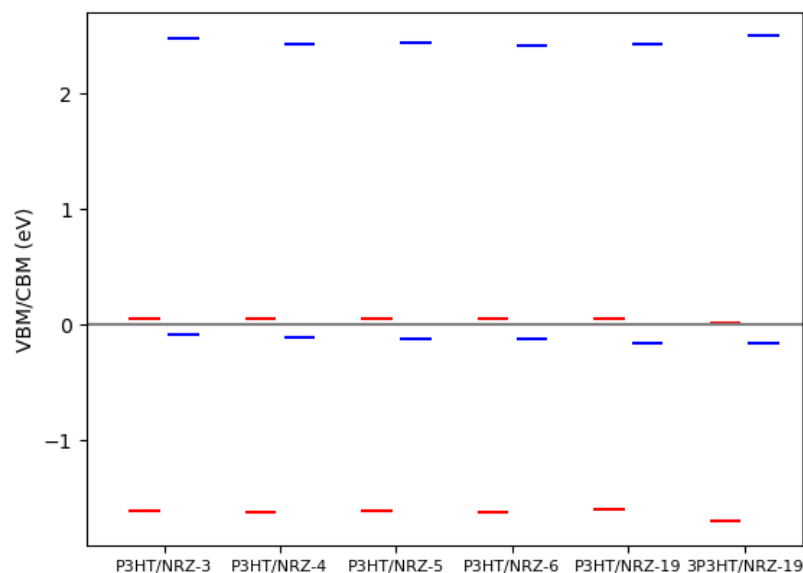


Figure 8. (Color online) The conduction and valence band alignments of heterostructures formed by edge-on P3HT 1D chain (red lines) and blue phosphorene zigzag nanoribbons (blue lines) of different widths. Calculations correspond to the use of DFT-1/2 approach.

4. Conclusions

We have investigated the electronic properties of semiconductor heterostructures of the P3HT blue phosphorene zigzag nanoribbon type in order to determine the kind of conduction and valence band alignment for their possible optoelectronic use. In accordance, P3HT periodic polymeric chain and blue phosphorene nanoribbons were separately studied using first principles within density functional theory. Different approaches, including GGA+PBE, HSE06 hybrid functional and DFT-1/2, were employed to determine the electronic dispersion relations and the energy band gaps of these compounds, with the main purpose of revealing the advantages of the DFT-1/2 approach, which is known as a quite accurate and computationally cheap method for dealing with the electronic properties of semiconductors.

According to our DFT-1/2 results, the 1D periodic P3HT polymeric chain is a direct gap semiconductor with $E_g = 1.62$ eV, and the blue phosphorene monolayer is an indirect gap semiconductor with $E_g = 1.97$ eV. However, blue phosphorene nanoribbons appear—barely—as indirect gap semiconductors, although the hybrid HSE06 approach results in a direct gap description in that case.

With such information at hand, the combination of both crystals to form a heterostructure produces a direct narrow gap complex, which, when analyzed from the point of view of band alignment, turns out to be a type-II semiconductor system. On the other hand, it would be interesting to consider the p-doping of the P3HT chain, as reported in [52], since convenient modifications of the electronic structure of the complex could be achieved. Work on this line is currently in progress.

Author Contributions: Authors contributed by performing the indicated activities: Conceptualization, J.D.C. and M.E.M.-R.; methodology, B.T.-C. and J.D.C.; software, B.T.-C. and J.D.C.; validation, J.D.C. and M.E.M.-R.; formal analysis, B.T.-C., J.D.C. and M.E.M.-R.; writing—review and editing, M.E.M.-R. and C.A.D. All authors have read and agreed to the published version of the manuscript.

Funding: This research was funded by Mexican CONACYT grant number A1-S-8218 (MEMR).

Data Availability Statement: Data are partially available through direct contact with the corresponding authors.

Conflicts of Interest: The authors declare no conflict of interest.

References

1. Geim, A.; Novoselov, K. The rise of graphene. *Nat. Mater.* **2007**, *6*, 183–191. [[CrossRef](#)] [[PubMed](#)]
2. Novoselov, K.; Jiang, D.; Schedin, F.; Booth, T.; Khotkevich, V.; Morozov, S.; Geim, A. Two-dimensional atomic crystals. *Proc. Natl. Acad. Sci. USA* **2005**, *102*, 10451–10453. [[CrossRef](#)] [[PubMed](#)]
3. Grazianetti, C.; Molle, A. Introduction. In *Xenes*; Molle, A., Grazianetti, C., Eds.; Woodhead Publishing Series in Electronic and Optical Materials; Woodhead Publishing: Cambridge, UK, 2022; pp. xxi–xxx. . [[CrossRef](#)]
4. Grazianetti, C.; Martella, C. The Rise of the Xenes: From the Synthesis to the Integration Processes for Electronics and Photonics. *Materials* **2021**, *14*, 4170. [[CrossRef](#)] [[PubMed](#)]
5. Kaur, S.; Kumar, A.; Srivastava, S.; Tankeshwar, K. Electronic structure engineering of various structural phases of phosphorene. *Phys. Chem. Chem. Phys.* **2016**, *18*, 18312–18322. [[CrossRef](#)]
6. Zhu, Z.; Tománek, D. Semiconducting layered blue phosphorus: A computational study. *Phys. Rev. Lett.* **2014**, *112*, 176802. [[CrossRef](#)]
7. Zhang, J.; Zhao, S.; Han, C.; Wang, Z.; Zhong, S.; Sun, S.; Guo, R.; Zhou, X.; Gu, C.; Yuan, K.; et al. Epitaxial growth of single layer blue phosphorus: A new phase of two-dimensional phosphorus. *Nano Lett.* **2016**, *16*, 4903–4908. [[CrossRef](#)]
8. Han, N.; Gao, N.; Zhao, J. Initial Growth Mechanism of Blue Phosphorene on Au(111) Surface. *J. Phys. Chem. C* **2017**, *121*, 17893–17899. [[CrossRef](#)]
9. Zhuang, J.; Liu, C.; Gao, Q.; Liu, Y.; Feng, H.; Xu, X.; Wang, J.; Zhao, J.; Dou, S.; Hu, Z.; et al. Bandgap Modulated by Electronic Superlattice in Blue Phosphorene. *ACS Nano* **2018**, *12*, 5059–5065. [[CrossRef](#)]
10. Zhang, W.; Enriquez, H.; Mayne, A.J.; Bendounan, A.; Seitsonen, A.; Kara, A.; Dujardin, G.; Oughaddou, H. First steps of blue phosphorene growth on Au(111). *Mater. Today Proc.* **2021**, *39*, 1153–1156. [[CrossRef](#)]
11. Shaikh, G.A.; Raval, D.; Babariya, B.; Gupta, S.; Gajjar, P. An ab-initio study of blue phosphorene monolayer: Electronic, vibrational and optical properties. *Mater. Today Proc.* **2021**, *47*, 576–579. [[CrossRef](#)]
12. Tyagi, S.; Rout, P.; Schwingenschlogl, U. High-performance junction-free field-effect transistor based on blue phosphorene. *npj 2D Mater. Appl.* **2022**, *6*, 86. [[CrossRef](#)]
13. He, C.; Xu, S.; Dong, X.; He, C.; Hu, X.; Liu, G.; Xu, H. Step-guided epitaxial growth of blue phosphorene on vicinal Ag(111). *Phys. Rev. Mater.* **2023**, *7*, 034003. [[CrossRef](#)]
14. Xie, J.; Si, M.; Yang, D.; Zhang, Z.; Xue, D. A theoretical study of blue phosphorene nanoribbons based on first-principles calculations. *J. Appl. Phys.* **2014**, *116*, 073704. [[CrossRef](#)]
15. Liu, Y.; Zhang, X.; Yang, X.; Hong, X.; Feng, J.; Si, M.; Wang, X. Spin caloritronics of blue phosphorene nanoribbons. *Phys. Chem. Chem. Phys.* **2015**, *17*, 10462–10467. [[CrossRef](#)] [[PubMed](#)]
16. Ospina, D.; Duque, C.; Mora-Ramos, M.; Correa, J. Effects of external electric field on the optical and electronic properties of blue phosphorene nanoribbons: A DFT study. *Comput. Mater. Sci.* **2017**, *135*, 43–53. [[CrossRef](#)]
17. Xiong, P.Y.; Chen, S.Z.; Zhou, W.X.; Chen, K.Q. Semiconductor-metal transition induced by giant Stark effect in blue phosphorene nanoribbons. *Phys. Lett. A* **2017**, *381*, 2016–2020. [[CrossRef](#)]
18. Swaroop, R.; Ahluwalia, P.; Tankeshwar, K.; Kumar, A. Ultra-narrow blue phosphorene nanoribbons for tunable optoelectronics. *RSC Adv.* **2017**, *7*, 2992–3002. [[CrossRef](#)]
19. An, Y.; Sun, Y.; Zhang, M.; Jiao, J.; Wu, D.; Wang, T.; Wang, K. Tuning the Electronic Structures and Transport Properties of Zigzag Blue Phosphorene Nanoribbons. *IEEE Trans. Electron Devices* **2018**, *65*, 4646–4651. [[CrossRef](#)]
20. Dey, A.; Chakraborty, D. Engineering the Band Structures of Zigzag Blue Phosphorene and Arsenene Nanoribbons by Incorporating Edge Corrugations: A First Principles Exploration. *J. Nanosci. Nanotechnol.* **2021**, *21*, 5929–5936. [[CrossRef](#)]
21. Saravanan, S.; Nagarajan, V.; Srivastava, A.; Chandiramouli, R. Blue phosphorene nanoribbon for detection of chloroform vapours—A first-principles study. *Int. J. Environ. Anal. Chem.* **2019**, *101*, 1697–1709. . [[CrossRef](#)]
22. Maibam, A.; Chakraborty, D.; Joshi, K.; Krishnamurty, S. Exploring edge functionalised blue phosphorene nanoribbons as novel photocatalysts for water splitting. *New J. Chem.* **2021**, *45*, 3570–3580. [[CrossRef](#)]
23. Macdonald, T.; Clancy, A.; Xu, W.; Jiang, Z.; Lin, C.T.; Mohan, L.; Du, T.; Tune, D.; Lanzetta, L.; Min, G.; et al. Phosphorene Nanoribbon-Augmented Optoelectronics for Enhanced Hole Extraction. *J. Am. Chem. Soc.* **2021**, *143*, 21549–21559. [[CrossRef](#)] [[PubMed](#)]
24. Sun, M.; Tang, W.; Ren, Q.; Wang, S.; Yu, J.; Du, Y. A first-principles study of light non-metallic atom substituted blue phosphorene. *Appl. Surf. Sci.* **2015**, *356*, 110–114. [[CrossRef](#)]
25. Ding, Y.; Wang, Y. Structural, electronic, and magnetic properties of adatom adsorptions on black and blue phosphorene: A first-principles study. *J. Phys. Chem. C* **2015**, *119*, 10610–10622. [[CrossRef](#)]
26. Sun, M.; Hao, Y.; Ren, Q.; Zhao, Y.; Du, Y.; Tang, W. Tuning electronic and magnetic properties of blue phosphorene by doping Al, Si, As and Sb atom: A DFT calculation. *Sol. Stat. Commun.* **2016**, *242*, 36–40. [[CrossRef](#)]

27. Bai, R.; Chen, Z.; Gou, M.; Zhang, Y. A first-principles study of group IV and VI atoms doped blue phosphorene. *Sol. Stat. Commun.* **2018**, *270*, 76–81. [[CrossRef](#)]
28. Arif Khalil, R.; Hussain, F.; Hussain, M.; Parveen, A.; Imran, M.; Murtaza, G.; Sattar, M.; Rana, A.; Kim, S. The investigation of optoelectronic, magnetic and dynamical properties of Ce and Ti doped 2D blue phosphorene: A dispersion corrected DFT study. *J. Alloys Compd.* **2020**, *827*, 154255. [[CrossRef](#)]
29. Correa, J. First principles calculations of opto-electronic properties of doped blue phosphorene nanoribbons. *Superlattices Microstruct.* **2019**, *130*, 401–408. [[CrossRef](#)]
30. Ihn, K.; Moulton, J.; Smith, P. Whiskers of poly(3-alkylthiophene)s. *J. Polym. Sci. B Polym. Phys.* **1993**, *31*, 735–742. [[CrossRef](#)]
31. Jian, L.; Bao, X.; Uchida, Y.; Liu, J.; Kathuria, Y.; Furuhashi, H.; Uchida, Y. Blue spectral shift of P3HT organic film by KrF excimer laser ablation. In Proceedings of the 2009 International Conference on Optical Instruments and Technology: Optoelectronic Devices and Integration, Shanghai, China, 19–21 October 2009; Zhang, X., Bock, W., Lu, X., Ming, H., Eds.; International Society for Optics and Photonics: Bellingham, WA, USA, 2009; Volume 7509, p. 75090F. [[CrossRef](#)]
32. Moulé, A.J.; Neher, D.; Turner, S. P3HT-Based Solar Cells: Structural Properties and Photovoltaic Performance. In *P3HT Revisited—From Molecular Scale to Solar Cell Devices*; Ludwigs, S., Ed.; Springer: Berlin/Heidelberg, Germany, 2014; pp. 181–232. [[CrossRef](#)]
33. El Gemayel, M.; Narita, A.; Dössel, L.F.; Sundaram, R.S.; Kiersnowski, A.; Pisula, W.; Hansen, M.R.; Ferrari, A.C.; Orgiu, E.; Feng, X.; et al. Graphene nanoribbon blends with P3HT for organic electronics. *Nanoscale* **2014**, *6*, 6301–6314. [[CrossRef](#)]
34. Tiwari, S.; Verma, R.; Alam, M.; Kumari, R.; Sinha, O.; Srivastava, R. Charge transport study of P3HT blended MoS₂. *Vacuum* **2017**, *146*, 474–477. [[CrossRef](#)]
35. Gutiérrez-González, I.; Molina-Brito, B.; Götz, A.W.; Castillo-Alvarado, F.; Rodríguez, J.I. Structural and electronic properties of the P3HT-PCBM dimer: A theoretical Study. *Chem. Phys. Lett.* **2014**, *612*, 234–239. [[CrossRef](#)]
36. Roy, J.K.; Kar, S.; Leszczynski, J. Optoelectronic Properties of C60 and C70 Fullerene Derivatives: Designing and Evaluating Novel Candidates for Efficient P3HT Polymer Solar Cells. *Materials* **2019**, *12*, 2282. [[CrossRef](#)] [[PubMed](#)]
37. Nguyen, T.P.; Shim, J.H. Hybrid density functional study on the electronic structures and properties of P3HT-PbS and P3HT-CdS hybrid interface for photovoltaic applications. *J. Comput. Chem.* **2018**, *39*, 1990–1999. [[CrossRef](#)] [[PubMed](#)]
38. Garcia-Basabe, Y.; Orsi Gordo, V.; Daminelli, L.; Mendoza, C.D.; Vicentin, F.; Matusalem, F.; Rocha, A.; de Matos, C.; Larrudé, D. Interfacial electronic coupling and band alignment of P3HT and exfoliated black phosphorous van der Waals heterojunctions. *Appl. Surf. Sci.* **2021**, *541*, 148455. [[CrossRef](#)]
39. Ferreira, L.; Marques, M.; Teles, L. Approximation to density functional theory for the calculation of band gaps of semiconductors. *Phys. Rev. B* **2008**, *78*, 125116. [[CrossRef](#)]
40. Ferreira, L.; Marques, M.; Teles, L. Slater half-occupation technique revisited: The LDA-1/2 and GGA-1/2 approaches for atomic ionization energies and band gaps in semiconductors. *AIP Adv.* **2011**, *1*, 032119. [[CrossRef](#)]
41. Slater, J.; Johnson, K. Self-Consistent-Field X_α Cluster Method for Polyatomic Molecules and Solids. *Phys. Rev. B* **1972**, *5*, 844–853. [[CrossRef](#)]
42. Slater, J. Statistical Exchange-Correlation in the Self-Consistent Field. *Adv. Quantum Chem.* **1972**, *6*, 1–92. [[CrossRef](#)]
43. Soler, J.; Artacho, E.; Gale, J.; García, A.; Junquera, J.; Ordejón, P.; Sánchez-Portal, D. The SIESTA method for ab initio order-N materials simulation. *J. Phys. Condens. Matter* **2002**, *14*, 2745. [[CrossRef](#)]
44. Artacho, E.; Anglada, E.; Diéguez, O.; Gale, J.; García, A.; Junquera, J.; Martin, R.; Ordejón, P.; Pruneda, J.; Sánchez-Portal, D.; et al. The SIESTA method; developments and applicability. *J. Phys. Condens. Matter* **2008**, *20*, 064208. [[CrossRef](#)] [[PubMed](#)]
45. Perdew, J.P.; Burke, K.; Ernzerhof, M. Generalized Gradient Approximation Made Simple. *Phys. Rev. Lett.* **1996**, *77*, 3865–3868. [[CrossRef](#)] [[PubMed](#)]
46. Heyd, J.; Scuseria, G.E. Efficient hybrid density functional calculations in solids: Assessment of the Heyd-Scuseria-Ernzerhof screened Coulomb hybrid functional. *J. Chem. Phys.* **2004**, *121*, 1187–1192. [[CrossRef](#)] [[PubMed](#)]
47. Heyd, J.; Peralta, J.E.; Scuseria, G.E.; Martin, R.L. Energy band gaps and lattice parameters evaluated with the Heyd-Scuseria-Ernzerhof screened hybrid functional. *J. Chem. Phys.* **2005**, *123*, 174101. [[CrossRef](#)] [[PubMed](#)]
48. Heyd, J.; Scuseria, G.E.; Ernzerhof, M. Erratum: “Hybrid functionals based on a screened Coulomb potential” [*J. Chem. Phys.* **118**, 8207 (2003)]. *J. Chem. Phys.* **2006**, *124*, 219906. [[CrossRef](#)]
49. Mortensen, J.J.; Hansen, L.B.; Jacobsen, K.W. Real-space grid implementation of the projector augmented wave method. *Phys. Rev. B* **2005**, *71*, 035109. [[CrossRef](#)]
50. Enkovaara, J.; Rostgaard, C.; Mortensen, J.J.; Chen, J.; Duřak, M.; Ferrighi, L.; Gavnholt, J.; Glinzvad, C.; Haikola, V.; Hansen, H.A.; et al. Electronic structure calculations with GPAW: A real-space implementation of the projector augmented-wave method. *J. Phys. Condens. Matter* **2010**, *22*, 253202. [[CrossRef](#)]
51. Marsman, M.; Paier, J.; Stroppa, A.; Kresse, G. Hybrid functionals applied to extended systems. *J. Phys. Condens. Matter* **2008**, *20*, 064201. [[CrossRef](#)]
52. Ansari, M.A.; Mohiuddin, S.; Kandemirli, F.; Malik, M.I. Synthesis and characterization of poly(3-hexylthiophene): Improvement of regioregularity and energy band gap. *RSC Adv.* **2018**, *8*, 8319–8328. [[CrossRef](#)]
53. Kucur, E.; Riegler, J.; Urban, G.A.; Nann, T. Charge transfer mechanism in hybrid bulk heterojunction composites. *J. Chem. Phys.* **2004**, *120*, 1500–1505. [[CrossRef](#)]

54. Cook, S.; Katoh, R.; Furube, A. Ultrafast studies of charge generation in PCBM: P3HT blend films following excitation of the fullerene PCBM. *J. Phys. Chem. C* **2009**, *113*, 2547–2552. [[CrossRef](#)]
55. Zhang, S.; Xie, M.; Li, F.; Yan, Z.; Li, Y.; Kan, E.; Liu, W.; Chen, Z.; Zeng, H. Semiconducting Group 15 Monolayers: A Broad Range of Band Gaps and High Carrier Mobilities. *Angew. Chem. Int. Ed.* **2016**, *55*, 1666–1669. [[CrossRef](#)] [[PubMed](#)]
56. Zhang, S.; Guo, S.; Chen, Z.; Wang, Y.; Gao, H.; Gómez-Herrero, J.; Ares, P.; Zamora, F.; Zhu, Z.; Zeng, H. Recent progress in 2D group-VA semiconductors: From theory to experiment. *Chem. Soc. Rev.* **2018**, *47*, 982–1021. . [[CrossRef](#)] [[PubMed](#)]

Disclaimer/Publisher's Note: The statements, opinions and data contained in all publications are solely those of the individual author(s) and contributor(s) and not of MDPI and/or the editor(s). MDPI and/or the editor(s) disclaim responsibility for any injury to people or property resulting from any ideas, methods, instructions or products referred to in the content.